Structural Engineering and Mechanics, Vol. 43, No. 5 (2012) 583-605
DOI: http://dx.doi.org/10.12989/sem.2012.43.5.583

Nonlinear analysis of cable-supported structures with a spatial catenary cable element

Tan-Van Vu*[1], Hak-Eun Lee[2] and Quoc-Tinh Bui[3]

[1]*Faculty of Civil Engineering, Ho Chi Minh City University of Architecture, Vietnam*
[2]*Civil, Environmental & Architectural Engineering, Korea University, 5-1, Anam-dong, Sungbuk-go, Seoul 136-701, Korea*
[3]*Department of Civil Engineering, University of Siegen, Germany*

(Received November 3, 2011, Revised May 31, 2012, Accepted August 9, 2012)

Abstract. This paper presents a spatial catenary cable element for the nonlinear analysis of cable-supported structures. An incremental-iterative solution based on the Newton-Raphson method is adopted for solving the equilibrium equation. As a result, the element stiffness matrix and nodal forces are determined, wherein the effect of self-weight and pretension are taken into account. In the case of the initial cable tension is given, an algorithm for form-finding of cable-supported structures is proposed to determine precisely the unstressed length of the cables. Several classical numerical examples are solved and compared with the other available numerical methods or experiment tests showing the accuracy and efficiency of the present elements.

Keywords: cable; cable-stayed bridge; catenary; geometric nonlinear analysis; nonlinear static analysis; cable pre-tension; long-span bridges; coupled flutter; multi-mode analysis; state space method

1. Introduction

Due to the importance of aesthetic appearance, efficient utilization of structural materials cables is widely used in engineering structures such as cable-supported bridges, cable roofs, guyed, towers/ masts and so on. Normally, the cable structures are highly flexible, they can undergo large deformation; hence geometric nonlinear effects should be taken account in the equilibrium equations. Recently, most of methods for analysis of realistic cable-supported structures are based on nite element methods, and can be grouped into two broad categories as follows: (i) the finite element approach (ii) the analytical approach. In the first approach, polynomials are employed to describe the shape and displacement field. Three different elements are developed based on this framework: straight bar elements, multi-node curved isoparametric bar elements, and curved elements with rotational degrees of freedom. The straight bar elements are commonly used in modeling the cables, which were adopted by several researchers (e.g., see Argyris and Scharpf 1972, Gambhir and Batchelor 1979, Ozdemir 1979). The sag effect of the cable can be considered by using equivalent stiffness (Ernst 1965), which is a function of the cable force, the self-weight of

*Corresponding author, Ph.D., E-mail: vvtanvan@korea.ac.kr

the cable, the length of the element and the axial stiffness of a straight cable. Since possessing only axial stiffness, these elements, on the one hand, are suitable for the representation of highly pretension cables; on the other hand, they are used when the cable lengths are sufficiently small. In case of slack cables with large curvature, a large number of bar elements are employed to represent the cable geometry. However, this strategy is inefficient because the number of degrees of freedom drastically increases. Due to the straight element assumption, one drawback can be encountered is the spurious slope discontinuities appearing at nodes where no concentrated loads act, and thus it may lead to numerical convergence problems. Instead of using many bar elements with linear interpolation functions one may use fewer multi-node curved isoparametric elements with higher order polynomials for the shape and displacements of the elements (Coyette and Guisset 1988, Ali and Abdel-Ghaffar 1995, Chen *et al.* 2010, Liu and Chen 2012). The tangent stiffness matrix and equivalent nodal forces are expressed in term of the isoparametric formulation and must be found by numerical integration. Accordingly, it will have a potential problem of convergence in the iteration course. Among those elements, the three- and four-node elements, which use parabolic and cubic interpolation functions, respectively, are commonly employed; hence, the out-of-plane response of the cable can be captured. Nevertheless, these curved elements give accurate results for cables with small sag, and only the displacement continuity is ensured between element nodes. The continuity of the slopes can be enforced by taking account of rotational degrees of freedom to the cable nodes. Such an element was developed by Gambhir and Batchelor (1977). The displacement field and shape are approximated by cubic polynomials, and the continuity at the cable nodes is enforced by using tangential and normal displacement components, rotation and curvature. Using the curved element can avoid the enforced continuity of higher order derivatives of the comparison functions (e.g., change in curvature). In case of slack cables with large curvature, a large number of elements are needed to adequately model the cable, but in the contrary to the other elements as presented above, no slope discontinuities are appeared. Since rotational degrees of freedom are included in the elements, the total number of degrees of freedom is, thus increased.

The second approach is based on analytical formulae to take into account the effect of uniformly distributed force applied along the length of the cable. Two elements, each associated with a certain type of uniformly distributed loading, have used in practice; these are parabolic, elastic catenary element. In a parabolic element, the loading is uniformly distributed along the cable chord. In this case, the geometry of a catenary has been approached by means of the second degree polynomials. Several researchers, such as Cohen and Perrin (1957), Poskitt and Livesley (1963), Mollmann (1970) have developed cable structures analysis techniques based on this approach. In general, the geometry of a parabola is an acceptable approximation of that of a catenary cable, but errors may be existed because of a discrepancy in geometry. The fundamental formulation of the elastic catenary element based on the analytical solutions was proposed by O'Brien and Francis (1964). The first element was presented by Peyrot and Goulois (1979), wherein the tangent stiffness matrix is obtained by taking the inverse of the flexibility matrix. The formulation, however, seems less accurate caused by the neglect of the out-of-plane stiffness. Subsequently, Jayaraman and Knudson (1981) improved the formulation by including such out-of-plane tangent stiffness, which is carried out by the coordinate transformation techniques. Many researchers, such as Wang *et al.* (2003), Andreu *et al.* (2006), Yang and Tsay (2007), Such *et al.* (2009) have employed the catenary element for analysis the cable-supported structures. The main advantage by using the catenary elements lies in the fact that only one element is needed to model the static behavior of both slack and taut cables subjected to uniformly distributed loads with a high degree of accuracy, and no discontinuities occur

at the element boundaries. It is worth noting that the consistent mass matrices are not available for the catenary elements, the analysis of the cable-supported structures under dynamic loads is thus required a refined technique to obtain more accurate results (Tibert 1998, Karoumi 1999). Nevertheless, this subject is beyond the scope of the present research work and is not addressed in this paper.

In this paper, a spatial catenary cable element is developed for the geometrical nonlinear analysis of cable-supported structures. The equilibrium equations of the proposed element are expressed in the final deformed configuration of the cable, the accurate treatment of the equilibrium is thus assured. It should be pointed that both in-of-plane and out-of-plane tangent stiffness matrices of the element are derived directly from a set of analytical expressions. An incremental-iterative solution based on the Newton-Raphson method is adopted for solving the implicit relationships between the nodal forces and displacements. In addition, a form-finding algorithm for nonlinear analysis of the cable unstressed length in case of given pre-tension force is presented. The accuracy and the efficiency of the proposed element are first validated through three benchmark numerical examples in comparison with other cable elements. Furthermore, to demonstrate the reliability of the proposed spatial catenary cable element, another engineering application in the framework of aerodynamic instability analysis for a long span bridge under an approaching crosswind is also shown.

The layout of the paper is as follows. The following section describes the derivation of the stiffness matrix and nodal forces for the spatial two-node catenary cable element. The aeroelastic flutter analysis of the long-span bridges is briefly introduced in section 3. Numerical comparative studies are presented in detail in Section 4, while the engineering application of the proposed cable element is discussed in Section 5. Finally, some concluding remarks are drawn from this work.

2. Formulation of spatial catenary cable element

2.1 Basic assumptions

The catenary cable element to be presented in this paper is derived based on the differential equations for a cable which is perfectly flexible with the self-weight distributed along its length and with the cross sectional area of the cable remaining constant. The element can be used for any sag-to-span ratio and both very slack and taut cables can be analyzed. The present formulation is based on the following basic assumptions:

(i) Only small deformation, but large displacement is considered.
(ii) Behavior of the cable is assumed linear-elastic constitutive
(iii) The cable is only subjected to its own weight, and conservation of the mass of the cable during the deformation process is assumed
(iv) Only the axial strain of the cable is considered, and its bending stiffness is neglected.

2.2 Equations of the spatial catenary cable element

Fig. 1 shows the elastic cable suspended between two nodes of I and J that have the Cartesian coordinates of $(0, 0, 0)$ and (L_x, L_y, L_z), respectively; the Lagragian coordinates for the undeformed and deformed configurations are s and p, respectively. With reference to the free body diagram in Fig. 1, the horizontal, lateral and vertical equilibrium conditions of the cable are

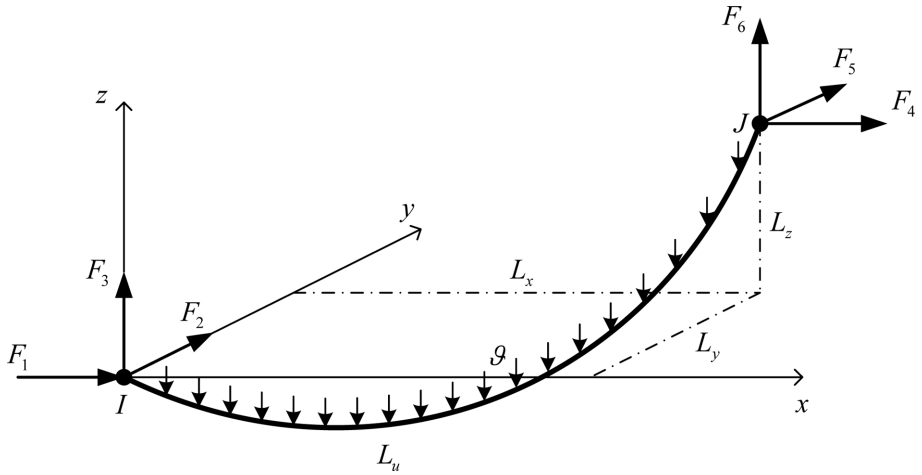

Fig. 1 Spatial catenary cable element

$$T\left(\frac{dx}{dp}\right) = -F_1 \tag{1a}$$

$$T\left(\frac{dy}{dp}\right) = -F_2 \tag{1b}$$

$$T\left(\frac{dz}{dp}\right) = -F_3 + \vartheta s \tag{1c}$$

where F_1, F_2 and F_3 are the horizontal, lateral and vertical components of the cable tension in the x-, y- and z-axis, respectively; and ϑ indicates the self-weight of the cable. From the equilibrium equations in Eq. (1), the cable tension T can be solved in terms of the Lagrangian coordinate, s as

$$T(s) = \sqrt{F_1^2 + F_2^2 + (-F_3 + \vartheta s)^2} \tag{2}$$

by noting that $dp^2 = dx^2 + dy^2 + dz^2$. Assuming that Hooke's law is applicable to the cable material, the constitutive relation of cable tension T and relative strain ε is,

$$T(s) = EA\varepsilon(s) = EA\left(\frac{dp}{ds} - 1\right) \tag{3}$$

where E and A are the elastic modulus and cross-sectional area of the cable, respectively. The Lagrangian coordinate is related to the Cartesian coordinate as follows

$$x(s) = \int \frac{dx}{ds} ds = \int \frac{dx}{dp}\frac{dp}{ds} ds \tag{4a}$$

$$y(s) = \int \frac{dy}{ds} ds = \int \frac{dy}{dp}\frac{dp}{ds} ds \tag{4b}$$

$$z(s) = \int \frac{dz}{ds} ds = \int \frac{dz}{dp}\frac{dp}{ds} ds \tag{4c}$$

and the boundary conditions at the catenary cable ends are

$$x(0) = y(0) = z(0) = 0 \tag{5a}$$

$$x(L_u) = L_x, \quad y(L_u) = L_y, \quad z(L_u) = L_z \tag{5b}$$

Substituting Eqs. (1)-(3) into Eq. (4) and imposing the boundary conditions in Eq. (5), and noting that a logarithmic representation is used for convenience as follows

$$\ln[(\cdot) + \sqrt{(\cdot)^2 + 1}] = \operatorname{arcsinh}(\cdot) \tag{6}$$

After some algebraic manipulations, the horizontal, lateral and vertical projection lengths L_x, L_y, L_z of the cable can be obtained.

$$L_x = -F_1\left\{\frac{L_u}{EA} + \frac{1}{\vartheta}\left[\operatorname{arcsinh}\left(\frac{\vartheta L_u - F_3}{\sqrt{F_1^2 + F_2^2}}\right) + \operatorname{arcsinh}\left(\frac{F_3}{\sqrt{F_1^2 + F_2^2}}\right)\right]\right\} \tag{7a}$$

$$L_y = -F_2\left\{\frac{L_u}{EA} + \frac{1}{\vartheta}\left[\operatorname{arcsinh}\left(\frac{\vartheta L_u - F_3}{\sqrt{F_1^2 + F_2^2}}\right) + \operatorname{arcsinh}\left(\frac{F_3}{\sqrt{F_1^2 + F_2^2}}\right)\right]\right\} \tag{7b}$$

$$L_z = \frac{\vartheta L_u^2}{EA}\left[\frac{1}{2} - \frac{F_3}{\vartheta L_u}\right] + \frac{1}{\vartheta}\left[\sqrt{F_1^2 + F_2^2 + (\vartheta L_u - F_3)^2} - \sqrt{F_1^2 + F_2^2 + F_3^2}\right] \tag{7c}$$

where L_u is unstressed length of the cable. The total length of the deformed catenary cable is given by the sum of the unstressed length L_u and the total elongation ΔL

$$L = L_u + \Delta L = L_u + \int \frac{T(s)}{EA} ds \tag{8}$$

Using the relation in Eq. (2), also applying the boundary conditions in Eq. (5) and using the logarithmic representation Eq. (6), then after manipulating we obtain the expression for the total length of the cable

$$L = L_u + \frac{1}{2EA\vartheta}\left\{\begin{array}{l} F_3\sqrt{F_1^2 + F_2^2 + F_3^2} + (\vartheta L_u - F_3)\sqrt{F_1^2 + F_2^2 + (F_3 - \vartheta L_u)^2} + \\ + (F_1^2 + F_2^2)\left[\operatorname{arcsinh}\left(\frac{\vartheta L_u - F_3}{\sqrt{F_1^2 + F_2^2}}\right) + \operatorname{arcsinh}\left(\frac{F_3}{\sqrt{F_1^2 + F_2^2}}\right)\right] \end{array}\right\} \tag{9}$$

The cable tension at nodes I and J is defined as

$$T_I = \sqrt{F_1^2 + F_2^2 + F_3^2} \tag{10a}$$

$$T_J = \sqrt{F_4^2 + F_5^2 + F_6^2} \tag{10b}$$

wherein the nodal forces at node J are F_4, F_5 and F_6, they can be obtained from static equilibrium equations

$$F_4 = -F_1 \tag{11a}$$

$$F_5 = -F_2 \tag{11b}$$

$$F_6 = -F_3 + \vartheta L_u \tag{11c}$$

It can be seen that the total length L and projection lengths L_x, L_y, L_z are also functions of the horizontal, lateral and vertical tension components, respectively i.e., $L = o(F_1, F_2, F_3)$ $L_x = p(F_1, F_2, F_3)$, $L_y = q(F_1, F_2, F_3)$ and $L_x = r(F_1, F_2, F_3)$. By differentiating both sides of Eq. (7) and using Eq. (6) then rewriting the results using matrix notation, the total differentials of the projection lengths can be expressed as

$$\begin{Bmatrix} dL_x \\ dL_y \\ dL_z \end{Bmatrix} = \begin{bmatrix} \frac{\partial p}{\partial F_1} & \frac{\partial p}{\partial F_2} & \frac{\partial p}{\partial F_3} \\ \frac{\partial q}{\partial F_1} & \frac{\partial q}{\partial F_2} & \frac{\partial q}{\partial F_3} \\ \frac{\partial r}{\partial F_1} & \frac{\partial r}{\partial F_2} & \frac{\partial r}{\partial F_3} \end{bmatrix} \begin{Bmatrix} dF_1 \\ dF_2 \\ dF_3 \end{Bmatrix} = \begin{bmatrix} f_{11} & f_{12} & f_{13} \\ f_{21} & f_{22} & f_{23} \\ f_{31} & f_{32} & f_{33} \end{bmatrix} \begin{Bmatrix} dF_1 \\ dF_2 \\ dF_3 \end{Bmatrix} = [F] \begin{Bmatrix} dF_1 \\ dF_2 \\ dF_3 \end{Bmatrix} \tag{12}$$

wherein the coefficients f_{ij} in the flexibility matrix $[F]$ are given as follows

$$f_{11} = -\frac{L_u}{EA} - \frac{1}{\vartheta}\left[\operatorname{arcsinh}\left(\frac{\vartheta L_u - F_3}{\sqrt{F_1^2 + F_2^2}}\right) + \operatorname{arcsinh}\left(\frac{F_3}{\sqrt{F_1^2 + F_2^2}}\right)\right] + \frac{F_1^2}{\vartheta(F_1^2 + F_2^2)} \times \left[\frac{\vartheta L_u - F_3}{T_J} + \frac{F_3}{T_I}\right] \tag{13}$$

$$f_{12} = \frac{F_1 F_2}{\vartheta(F_1^2 + F_2^2)}\left[\frac{\vartheta L_u - F_3}{T_J} + \frac{F_3}{T_I}\right], \quad f_{13} = \frac{F_1}{\vartheta}\left[\frac{1}{T_J} - \frac{1}{T_I}\right], \quad f_{21} = f_{12} \tag{14a, 14b, 14c}$$

$$f_{22} = -\frac{L_u}{EA} - \frac{1}{\vartheta}\left[\operatorname{arcsinh}\left(\frac{\vartheta L_u - F_3}{\sqrt{F_1^2 + F_2^2}}\right) + \operatorname{arcsinh}\left(\frac{F_3}{\sqrt{F_1^2 + F_2^2}}\right)\right] + \frac{F_2^2}{\vartheta(F_1^2 + F_2^2)} \times \left[\frac{\vartheta L_u - F_3}{T_J} + \frac{F_3}{T_I}\right] \tag{15}$$

$$f_{23} = \frac{F_2}{\vartheta}\left[\frac{1}{T_J} - \frac{1}{T_I}\right], \quad f_{31} = f_{13}, \quad f_{32} = f_{23}, \quad f_{33} = -\frac{L_u}{EA} - \frac{1}{\vartheta}\left[\frac{\vartheta L_u - F_3}{T_J} + \frac{F_3}{T_I}\right] \tag{16a, 16b, 16c, 16d}$$

The tangent local stiffness matrix $[K_{LC}]$ of a cable relates to the small changes in the end forces due to small end displacements, or

$$[K_{LC}] = \begin{bmatrix} -[\Xi] & [\Xi] \\ [\Xi] & -[\Xi] \end{bmatrix}, \quad \text{with} \quad [\Xi] = [F]^{-1} = \begin{bmatrix} f_{11} & f_{12} & f_{13} \\ f_{21} & f_{22} & f_{23} \\ f_{31} & f_{32} & f_{33} \end{bmatrix}^{-1} \tag{17}$$

The end forces can be stored in the local force vector as

$$\{F_{LC}\} = \{F_1, F_2, F_3, F_4, F_5, F_6\}^T \tag{18}$$

Once the tangent stiffness matrix and end forces vector are obtained, the cable length is estimated as (O'Brien and Francis 1964)

$$L = \sqrt{L_z^2 + (L_x^2 + L_y^2)\frac{\sinh^2\lambda}{\lambda^2}}, \quad \text{with} \quad \lambda = \frac{\vartheta}{2}\sqrt{\frac{L_x^2 + L_y^2}{F_1^2 + F_2^2}} \tag{19a, 19b}$$

2.3 Algorithm for computing the stiffness matrix element and end forces

The tangent stiffness element and nodal forces of the spatial catenary cable element are calculated using an iteration method. Based on the catenary relationships, the following expressions will be used for evaluating the initial values of the end forces (F_1, F_2, F_3) (Jayaraman and Knudson 1981)

$$F_1 = -\frac{\vartheta L_{0x}}{2\lambda_0} \tag{20a}$$

$$F_2 = -\frac{\vartheta L_{0y}}{2\lambda_0} \tag{20b}$$

$$F_3 = -\frac{\vartheta}{2}\left(L_{0z}\frac{\cosh\lambda_0}{\sinh\lambda_0} - L_u\right) \tag{20c}$$

where L_{0x}, L_{0y} and L_{0z} are initial projection lengths of the cable element, while a constant of λ_0 is estimated as follows. A value of 0.2 is assumed for λ_0 when the unstressed length L_u of the cable is shorter than the chord length, i.e., $(L_{x0} + L_{y0} + L_{z0})^{0.5}$, while an arbitrarily large value of 10^6 is adopted for λ_0 in the case of a vertical hanger, i.e., $(L_{x0}^2 + L_{y0}^2) = 0$; for other cases, the following is adopted (Peyrot and Goulois 1978)

$$\lambda_0 = \sqrt{3\left(\frac{L_u^2 - L_{z0}^2}{L_{x0}^2 + L_{y0}^2}\right)} \tag{21}$$

The tangent stiffness matrix and nodal force of the cable element are obtained by performing the iteration procedure briefly described as follows

- Step-1: Input ϑ, E, A, L_u, and the global coordinates $I(x_i, y_i, z_i)$ and $J(x_j, y_j, z_j)$
- Step-2: Calculate $L_{0x} = x_j - x_i$, $L_{0y} = y_j - y_i$ and $L_{0z} = z_j - z_i$
- Step-3: Initialize end forces $\{F\}^i = \{F_1\ F_2\ F_3\}_i^T$ using Eq. (20)
- Step-4: Calculate projection lengths (L_x, L_y, L_z) using Eq. (7)
- Step-5: Calculate the differences between the initial and computed projection lengths

$$dL = \{(L_{0x} - L_x)\ (L_{0x} - L_x)\ (L_{0x} - L_x)\}^T$$

- Step-6: If $|dL|$ is smaller than preset tolerance, calculate the element stiffness matrix $[K_{LC}]$ using Eq. (17) and nodal forces $\{F_{LC}\}$ using Eq. (18). Otherwise go to Step-7
- Step-7: Calculate the difference of nodal forces, $\{dF\} = [\Xi]\{dL\}$
- Step-8: Update the end forces $\{F\}^{i+1} = \{F\}^i + \{dF\}$, and go to Step-4.

Normally, the initial cable tension T_0 is given instead of the unstressed length L_u in terms of the variety the engineering applications. The relationship between the elongation and the tension force is

$$T = EA\frac{\Delta L}{L_u} = EA\frac{L - L_u}{L_u} \tag{22}$$

This equation can be written as

$$L_u = \frac{L}{T/AE + 1} \tag{23}$$

From Eq. (19) and Eq. (23), the relationship between the unstressed length and tension force is as follows

$$L_u = \frac{EA}{T + EA}\sqrt{L_z^2 + (L_x^2 + L_x^2)\frac{\sinh^2\lambda}{\lambda^2}} \tag{24}$$

In order to start the iteration one could use any good predict for initial value of L_u. However, the expression for unstressed length may be used (Karoumi 1999).

$$L_u = \sqrt{L_{0x}^2 + L_{0y}^2 + L_{0z}^2} \tag{25}$$

The iteration procedure for estimating the unstressed cable length is briefly summarized in the following steps

- Step-1: Input ϑ, E, A, T_0, and the global coordinates $I(x_i, y_i, z_i)$ and $J(x_j, y_j, z_j)$
- Step-2: Calculate $L_{0x} = x_j - x_i$, $L_{0y} = y_j - y_i$ and $L_{0z} = z_j - z_i$
- Step-3: Initialize unstressed length L_u using Eq. (23)
- Step-4: Initialize end forces $\{F\}^i = \{F_1\ F_2\ F_3\}_i^T$ using Eq. (20)
- Step-5: Calculate the differences between the projection lengths and tension forces

$$dL = \{(L_{0x} - L_x)\ (L_{0x} - L_x)\ (L_{0x} - L_x)\}^T \text{ and } dP = [T_0 - 0.5(T_I + T_J)]$$

- Step-6: If $|dL|$ and $|dP|$ are larger than the preset tolerance go to Step-7. Otherwise, calculate the total cable length L using Eq. (19), and the unstressed length L_u using Eq. (9), namely

$$L_u = L - \left\{F_3 T_I + F_6 T_J + (F_1^2 + F_2^2)\left[\operatorname{arcsinh}\left(\frac{F_6}{\sqrt{F_1^2 + F_2^2}}\right) + \operatorname{arcsinh}\left(\frac{F_3}{\sqrt{F_1^2 + F_2^2}}\right)\right]\right\} \tag{26}$$

- Step-7: Calculate the differences of nodal forces, $\{dF\} = [\Xi]\{dL\}$
- Step-8: Update the end forces $\{F\}^{i+1} = \{F\}^i + \{dF\}$
- Step-9: Update the unstressed length L_u as follows

$$L_u = \frac{EA}{T_0 + EA}\sqrt{L_{0z}^2 + (L_{0x}^2 + L_{0x}^2)\frac{\sinh^2\lambda}{\lambda^2}}, \quad \text{with} \quad \lambda = \frac{\vartheta}{2}\sqrt{\frac{L_{0x}^2 + L_{0y}^2}{F_1^2 + F_2^2}} \tag{27a, 27b}$$

and then go to Step-4.

3. Aerodynamic instability analysis of the long-span bridges

The self-excited forces per unit span of a bridge deck, arising from the interaction between the

smooth wind flow and the bridge, that include the lift force L_{ae}, drag force D_{ae} and pitching moment M_{ae} can be expressed as a linear combination of nodal displacement and velocity, and the entire complement of 18 flutter derivatives are given as Sarkar *et al.* (1994), Jain *et al.* (1996)

$$L_{ae} = \frac{1}{2}\rho U^2 B\left[KH_1^*\frac{\dot{h}}{U} + KH_2^*\frac{B\dot{\alpha}}{U} + K^2H_3^*\alpha + K^2H_4^*\frac{h}{B} + KH_5^*\frac{\dot{p}}{U} + K^2H_6^*\frac{p}{B}\right] \tag{28a}$$

$$D_{ae} = \frac{1}{2}\rho U^2 B\left[KP_1^*\frac{\dot{p}}{U} + KP_2^*\frac{B\dot{\alpha}}{U} + K^2P_3^*\alpha + K^2P_4^*\frac{p}{B} + KP_5^*\frac{\dot{h}}{U} + K^2P_6^*\frac{h}{B}\right] \tag{28b}$$

$$M_{ae} = \frac{1}{2}\rho U^2 B^2\left[KA_1^*\frac{\dot{h}}{U} + KA_2^*\frac{B\dot{\alpha}}{U} + K^2A_3^*\alpha + K^2A_4^*\frac{h}{B} + KA_5^*\frac{\dot{p}}{U} + K^2A_6^*\frac{p}{B}\right] \tag{28c}$$

where $A_i^*, H_i^*, P_i^* (i = \overline{1,6})$ are the non-dimensional flutter derivatives which are dependent upon the reduced frequency, $K(=B\omega/U)$, ρ is the air mass density, U is the wind velocity, $B = 2b$ is the bridge deck width, and ω is the circular frequency. h, p and α are the vertical, lateral and torsional displacement, respectively, and the dot indicates differentiation with respect to time. The motion-dependent aeroelastic forces and the heave, sway and torsional deformations are shown in their positive directions in Fig. 2.

Eq. (28) represents the real-number expressions for the aeroelastic forces. In complex notation, the corresponding expressions of the self-excited forces are (Starossek 1998, Ding *et al.* 2002)

$$L_{ae} = \omega^2\pi\rho b^2(C_{Lh}h + C_{Lp}p + bC_{L\alpha}\alpha) \tag{29a}$$

$$D_{ae} = \omega^2\pi\rho b^2(C_{Dh}h + C_{Dp}p + bC_{D\alpha}\alpha) \tag{29b}$$

$$M_{ae} = \omega^2\pi\rho b^2(bC_{Mh}h + bC_{Mp}p + b^2C_{M\alpha}\alpha) \tag{29c}$$

where $C_{rs}(r = D, L, M;\ s = h, p, \alpha)$ are the complex coefficients of self-excited forces. By comparing the aerodynamic force expressions in real and complex notation, these coefficients can

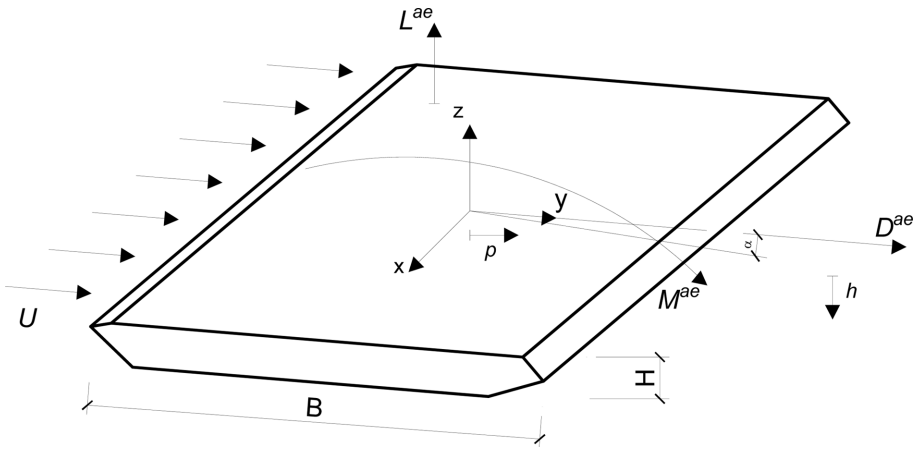

Fig. 2 Sign convention of aerodynamic forces and deformations for a bridge deck

be found as

$$C_{Lh} = \frac{2}{\pi}(H_4^* + iH_1^*), \quad C_{Lp} = \frac{2}{\pi}(H_6^* + iH_5^*), \quad C_{L\alpha} = \frac{4}{\pi}(H_3^* + iH_2^*) \tag{30a}$$

$$C_{Dh} = \frac{2}{\pi}(P_6^* + iP_5^*), \quad C_{Dp} = \frac{2}{\pi}(P_4^* + iP_1^*), \quad C_{D\alpha} = \frac{4}{\pi}(P_3^* + iP_2^*) \tag{30b}$$

$$C_{Mh} = \frac{4}{\pi}(A_4^* + iA_1^*), \quad C_{Mp} = \frac{4}{\pi}(A_6^* + iA_5^*), \quad C_{M\alpha} = \frac{8}{\pi}(A_3^* + iA_2^*) \tag{30c}$$

Although the two forms of self-excited forces are equivalent, it can be seen that the complex equations are more compact when comparing the real-notation force expressions (28) with the equivalent complex expressions (29). Obviously, the complex coefficients represent naturally the phasing between the displacements and displacement-induced aerodynamic forces. Meanwhile, the velocity terms $\dot{h}, \dot{p}$ and $\dot{\alpha}$ with the corresponding coefficients are included to properly account for phasing in real notation.

By considering the effects of inertia forces, damping forces, elastic forces and self-excited wind forces, the equations of equilibrium for the bridge can be written as

$$[M]\{\ddot{q}(t)\} + [C]\{\dot{q}(t)\} + [K]\{q(t)\} = \omega^2[A_{ae}]\{q(t)\} \tag{31}$$

Eq. (31) represents the mathematical model of the structural system under the effect of wind load, wherein $[M], [C], [K]$ are the structural mass, damping and stiffness matrices, respectively, and $\ddot{q}(t), \dot{q}(t), q(t)$ denote the structural displacement, velocity and acceleration vectors, respectively. $[A_{ae}]$ is a so-called aerodynamic matrix, of which the elements are derived by Vu (2010).

For a linear elastic structure, wherein the structure system is a very large value of degrees- of-freedoms, the commonly used modal superposition technique is employed to solve the equation of motion by using the first m-structural natural modes ($m \ll n$). Accordingly, the response in the displacement vector $\{q(t)\}$ can be approximated by

$$\{q(t)\} = [\Phi]\{y(t)\} \tag{32}$$

where $[\Phi]$ is the matrix of size $n \times m$ consisting of the mass-normalized mode shapes of selected m participating modes, and $\{y(t)\}$ denotes the mth-order vector of the generalized modal coordinate. Substituting Eq. (32) into Eq. (31), pre-multiplying $[\Phi]^T$, and then applying the orthogonal condition gives the representing modal-motion equations as

$$[I]\{\ddot{y}\} + [\hat{C}]\{\dot{y}\} + ([\hat{K}] - \omega^2[A_{ae}])\{y\} = \{0\} \tag{33}$$

where $[\hat{C}] = [\Phi]^T[C][\Phi] = diag(2\omega_1\xi_1, 2\omega_2\xi_2, \ldots, 2\omega_m\xi_m)$ represents the generalized Rayleigh damping matrix, $[\Lambda] = [\Phi]^T[K][\Phi] = diag(\omega_1^2, \omega_2^2, \ldots, \omega_m^2)$ denotes the diagonal matrix of eigenvalues, and $[\hat{A}_{ae}] = [\Phi]^T[A_{ae}][\Phi]$ indicates a generalized aerodynamic matrix.

Let the solution to Eq. (33) have the form $\{y(t)\} = \{\Delta^*\}e^{i\omega t}$, then the analysis of complex eigenvalues and eigenvectors of the system is converted into the following generalized eigenvalue problem (GEP) with $2m$-eigenvalues and eigenvectors, namely

$$[P^*][Z^*] = \eta[Q^*]\{Z^*\} \tag{34}$$

where

$$[P^*] = \begin{bmatrix} [\hat{C}] & [\Lambda] \\ [I^*] & [0^*] \end{bmatrix}, \quad [Q^*] = \begin{bmatrix} -[I^*]-[\hat{A}_{ae}] & [0^*] \\ [0^*] & [I^*] \end{bmatrix}, \quad \{Z\} = \begin{Bmatrix} \eta\Delta^* \\ \Delta^* \end{Bmatrix} \tag{35a, 35b, 35c}$$

in which $[I^*]$ and $[0^*]$ are the $m \times m$ identity and null matrix, respectively.

Eq. (34) depends on the reduced frequency, K and vibration frequency, ω. With this equation, a complex eigenvalue analysis process can be employed to determine the eigenvalues of the structural system as follows. When K is fixed, solving Eq. (34) yields conjugate pairs of complex eigenvalues, $\eta_j = \sigma_j \pm i\omega_j (j = \overline{1,n})$ and the conjugate pairs of complex eigenvectors, $Z_j = r_j \pm is_j (j = \overline{1,n})$ are obtained.

In the border case of onset flutter instability, the corresponding imaginary part of the complex eigenvalue η_f has a zero real part, and a positive imaginary part. Hence, K must be fixed repeatedly until this condition is met. The critical wind speed, $U_f = B\omega_f/K$, wherein ω_f is the flutter frequency. For the purpose of practical flutter prediction, the lowest possible wind speed resulting in the aeroelastic instability is most important and of concern. The algorithmic implementation for the full order analysis is summarized in the following steps (Vu *et al.* 2011):

(1) Compute the reduced frequency, K_j from within the range of $[0, K_{\max}]$ and a reduced frequency increment ΔK: $K_j = K_{j-1} + (j-1)\Delta K$

(2) Compute the flutter derivatives $A_i^{*(j)}, H_i^{*(j)}, P_i^{*(j)} (i = \overline{1,6})$ by the B-Spline interpolation technique, then construct the aerodynamic matrix, $[\mathbf{A}_{ae}^{(j)}]$

(3) Compute $\{\eta_j\}_{1\times n} = \{\mu_j + i\omega_j\}_{1\times n}$ from solving the GEP defined by Eq. (34);

(4) Loop over the rth complex modes $(r = \overline{1,n})$

If $[\mu_{j-1}^{(r)} \times \mu_j^{(r)}] \le 0$ or $|\mu_j^{(r)}| \le \varepsilon$, with $\varepsilon = 10^{-5}$ then,

- Compute the reduced frequency, $K_j^{f,(r)}$, and compute $\omega_j^{f,(r)}$ using the linear interpolation technique.

$$K_j^{f,(r)} = \frac{\mu_j^{(r)} K_{j-1} - \mu_{j-1}^{(r)} K_j}{\mu_j^{(r)} - \mu_{j-1}^{(r)}}, \quad \omega_j^{f,(r)} = \frac{\mu_j^{(r)} \omega_{j-1}^{(r)} - \mu_{j-1}^{(r)} \omega_j^{(r)}}{\mu_j^{(r)} - \mu_{j-1}^{(r)}} \tag{36a, 36b}$$

- Compute $U_j^{f,(r)} = B\omega_j^{f,(r)}/K_j^{f,(r)}$.

(5) Set $j = j + 1$:

If $K_j = K_{\max}$, go to Step (6), otherwise repeat Step (1) to Step (4)

(6) Compute the lowest onset flutter for each complex mode rth: $U_r^{f,\min} = \min_j \{U_j^{f,(r)}\}$ and $\omega_r^{f,\min} = \min_j \{\omega_j^{f,(r)}\}$ with $(j = \overline{1,n})$.

(7) Compute the lowest critical speed flutter; $U_r = \min\{U_j^{f,\min}\}$ and the flutter frequency $\omega_f = \min\{\omega_r^{f,\min}\}$ for all complex modes.

4. Numerical validations

In order to demonstrate the reliability and utility of the spatial catenary cable element presented

here, three simple problems have been chosen and the results are compared with those obtained by using other elements quoted in the literature. The well known Newton-Raphson method is employed for solving the nonlinear static analysis. The spatial catenary cable element with proposed algorithms has been incorporated in a FORTRAN program.

4.1 A single cable under a concentrated load

The isolated cable under self-weight and concentrated load shown in Fig. 3 is examined. The displacements of the load point are calculated. The cable is modeled by two catenary cable elements. This problem was first considered by Michalos and Birnstiel (1960), and later analyzed by O'Brien and Francis (1964), Jayaraman and Knudson (1981), Tibert (1998), Andreu *et al.* (2006), Yang and Tsay (2007). The data for this structure are presented in Table 1.

The results from the computations are shown in Table 2 together with the results obtained by other researchers. It can be clearly seen that the results obtained by the current cable element agree well with those predicted by other authors. It should be noted that elastic catenary type elements can achieve the same level of accuracy as that of the straight bar type element by using less elements.

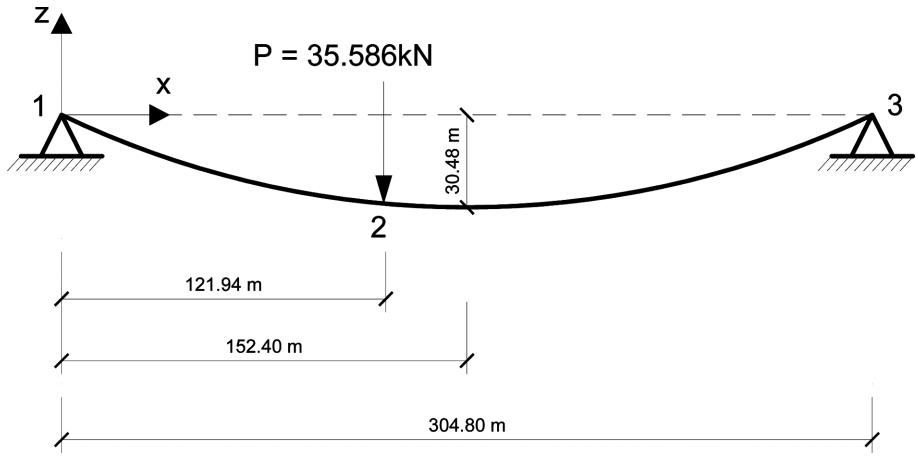

Fig. 3 A single cable under a concentrated load

Table 1 Initial Isolated cable properties under self-weight and concentrated load

Description		Magnitude
Cross-sectional area		5.484 cm^2
Elastic modulus		13,100 KN/cm^2
Self weight		46.120 N/m
Unstrained length	Segment 1-2	125.88 m
	Segment 2-3	186.850 m

Table 2 Displacement at load point for isolated cable

Investigator	Element type	Displacements (m)	
		Vertical	Horizontal
Saafan (1970)	Elastic straight	-5.472	-0.846
O'Brien and Francis (1964)	Elastic catenary	-5.627 (-2.83%)[a]	-0.860 (-1.65%)
Michalos and Birnstiel (1962)	Elastic straight	-5.472 (0.00%)	-0.845 (0.12%)
Jayaraman and Knudson (1981)	Elastic straight	-5.471 (0.02%)	-0.845 (0.12%)
Jayaraman and Knudson (1981)	Elastic catenary	-5.626 (-2.81%)	-0.859 (-1.54%)
Tibert (1998)	Elastic catenary	-5.626 (-2.81%)	-0.859 (-1.54%)
Tibert (1998)	Elastic parabola	-5.601 (-2.36%)	-0.866 (-2.36%)
Tibert (1998)	Associated catenary	-5.656 (-3.36%)	-0.860 (-1.65%)
Andreu et al. (2006)	Elastic catenary	-5.626 (-2.81%)	-0.860 (-1.65%)
Yang and Tsay (2007)	Elastic catenary	-5.626 (-2.81%)	-0.859 (-1.54%)
Present	Elastic catenary	-5.626 (-2.81%)	-0.859 (-1.54%)

[a]Numbers in parentheses are the percentage error with respect to Saafan (1970) values

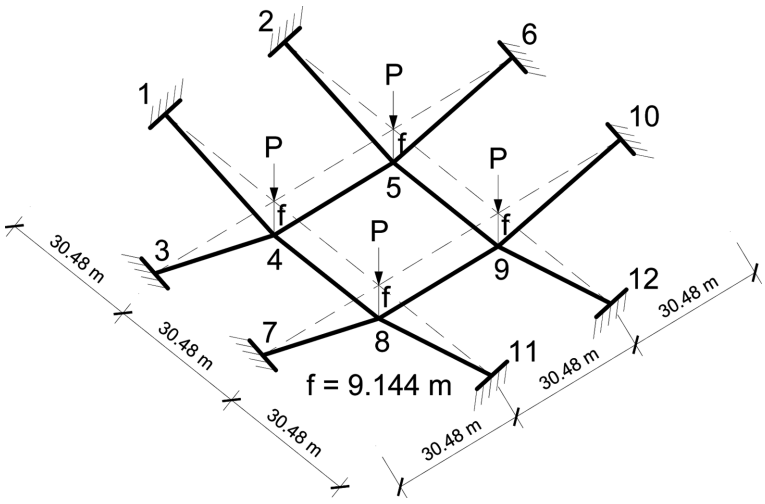

Fig. 4 A pre-stressed plane cable net

4.2 A pre-stressed cable net under vertical loads

The structure considered is the pre-stressed cable net shown in Fig. 4. This structure was first studied by Saafan (1970) and subsequently considered by West and Kar (1973), Jayaraman and Knudson (1981), Tibert (1998). Initial properties are given in Table 3. The vertical displacements of cable net at load point for structure are compared in Table 4. A good agreement can be seen between the displacements of the cable net predicted by the proposed program in this study and that predicted by the other authors.

Table 3 Initial properties of the cable net

Description		Magnitude
Cross-sectional area		146.45 mm^2
Elastic modulus		82,737 MPA
Self weight		1.459 N/m
Prestressing force	Horizontal members	24.283 KN
	Inclined members	23.687 KN
Load acting vertically downward at all internal nodes		35.586 KN

Table 4 Comparison of predict displacement of the cable net

Investigator	Element type	Displacements of node 1 (mm)		
		x-dir	*y*-dir	*z*-dir
Saafan (1970)	Elastic straight	-40.36	-40.36	-448.27
West and Kar (1973)	Elastic straight	-40.39 (-0.08%)[b]	-40.36 (0.00%)	-448.00 (0.06%)
Jayaraman and Knudson (1981)	Elastic straight	-39.62 (1.81%)	-40.20 (0.38%)	-446.32 (0.44%)
Jayaraman and Knudson (1981)	Elastic catenary	-40.29 (0.15%)	-40.29 (0.15%)	-448.27 (0.00%)
Tibert (1998)	Elastic catenary	-40.48 (-0.30%)	-40.48 (-0.30%)	-450.01 (-0.39%)
Tibert (1998)	Elastic parabola	-40.78 (-1.06%)	-40.78 (-1.06%)	-453.33 (-1.13%)
Tibert (1998)	Associated catenary	-40.78 (-1.06%)	-40.78 (-1.06%)	-453.36 (-1.14%)
Present	Elastic catenary	-40.47 (-0.29%)	-40.47 (-0.29%)	-449.42 (-0.26%)

[b]Numbers in parentheses are the percentage error with respect to Saafan (1970) values

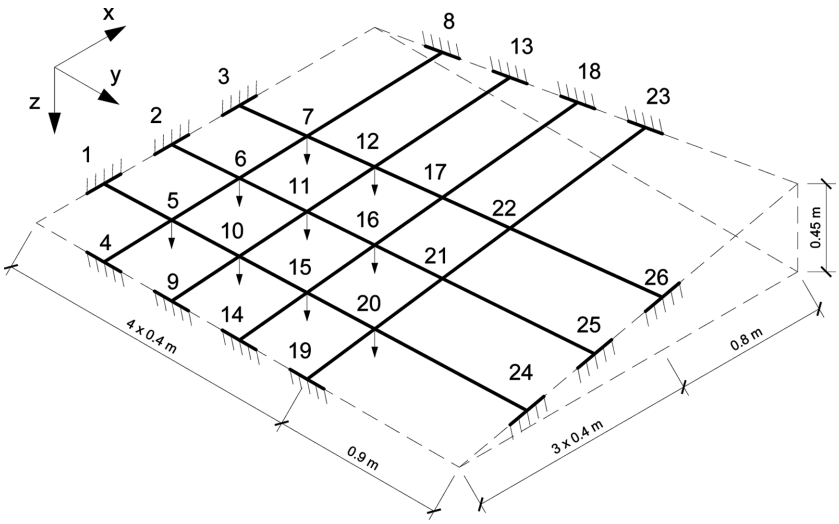

Fig. 5 Hyperbolic parabolid net

Table 5 Comparison of predict vertical displacement (mm) of the hypar net

Node	Experiment Lewis *et al.* (1984)	Rigidity matrix Krishna (1978)	Minimum energy Sufian and Templeman (1992)	Approximation by series Kwan (1998)	Andreu *et al.* (2006)	Present method
5	19.50	19.60 (-0.51%)[c]	19.30 (1.03%)	19.52 (-0.10%)	19.51 (-0.05%)	19.38 (0.63%)
6	25.30	25.90 (-2.37%)	25.50 (-0.79%)	25.35 (-0.20%)	25.65 (-1.38%)	25.39 (-0.36%)
7	22.80	23.70 (-3.95%)	23.10 (-1.32%)	23.31 (-2.24%)	23.37 (-2.50%)	23.09 (-1.27%)
10	25.40	25.30 (0.39%)	25.80 (-1.57%)	25.86 (-1.81%)	25.87 (-1.85%)	25.65 (-1.00%)
11	33.60	33.00 (1.79%)	34.00 (-1.19%)	34.05 (-1.34%)	34.14 (-1.61%)	33.72 (-0.36%)
12	28.80	28.20 (2.08%)	29.40 (-2.08%)	29.49 (-2.40%)	29.65 (-2.95%)	29.25 (-1.57%)
15	25.20	25.80 (-2.38%)	25.70 (-1.98%)	25.79 (-2.34%)	25.86 (-2.62%)	25.41 (-0.84%)
16	30.60	31.30 (-2.29%)	31.20 (-1.96%)	31.31 (-2.32%)	31.47 (-2.84%)	30.74 (-0.45%)
17	21.00	21.40 (-1.90%)	21.10 (-0.48%)	21.42 (-2.00%)	21.57 (-2.71%)	21.01 (-0.07%)
20	21.00	22.00 (-4.76%)	21.10 (-0.48%)	21.48 (-2.29%)	21.62 (-2.95%)	20.61 (1.87%)
21	19.80	21.10 (-6.57%)	19.90 (-0.51%)	20.00 (-1.01%)	20.15 (-1.77%)	18.88 (4.67%)
22	14.20	15.70 (-10.56%)	14.30 (-0.70%)	14.40 (-1.41%)	14.55 (-2.46%)	13.54 (4.62%)

[c]Numbers in parentheses are the percentage error with respect to experiment values

4.3 A hypar net under some vertical loads

The hypar net is generated by two sets of straight line cables as shown in Fig. 5. The model of the hyperbolic paraboloid surface was first investigated by Lewis *et al.* (1984) and then numerically analyzed by Sufian and Tempelman (1992). This cable network consists of 31 cable segments subjected to a concentrated load of 0.0157 KN at all internal nodes, except nodes 17, 21 and 22. The cross-section area and elastic modulus are 124.8 KN/mm^2 and 0.785 mm^2, respectively. The cable segments are pre-tensioned to carry 200.0 N prior to the application of external load.

Table 5 shows a comparison of the vertical displacements obtained by the present work with those predicted by the other authors using different numerical methods. It can be seen that the proposed element can accurately predict the behavior of the cable with the maximum difference of 4.67%.

5. An engineering application for aerodynamic instability analysis of cable-stayed bridge

In this section, the present spatial cable element is applied to the aerodynamic instability analysis of the New Millennium Bridge, an asymmetric cable-stayed bridge in the south-western region of Korea with a main span of 510.0 m (Fig. 6). The wind-tunnel tests of the section model and full

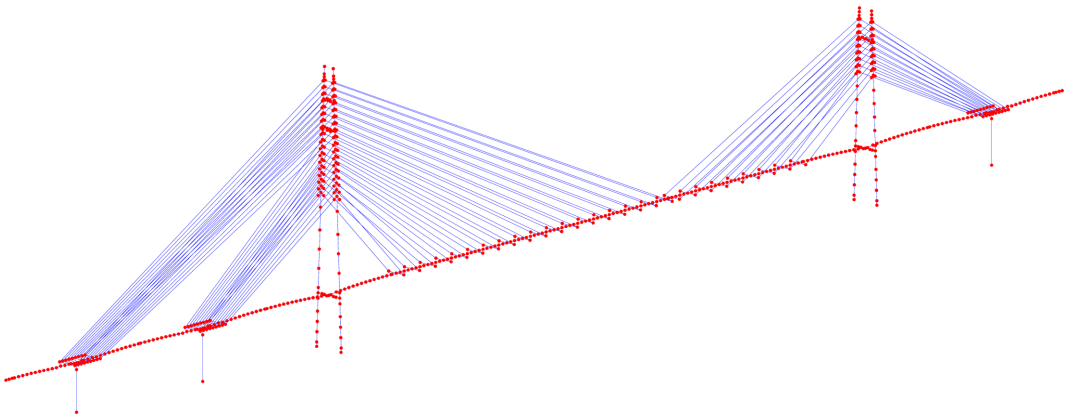

Fig. 6 Finite element model of the New Millennium bridge for flutter analysis

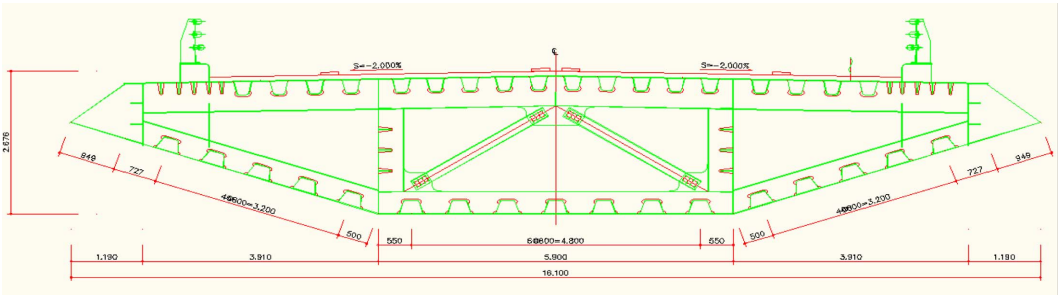

Fig. 7 Cross-section of deck of the New Millennium bridge

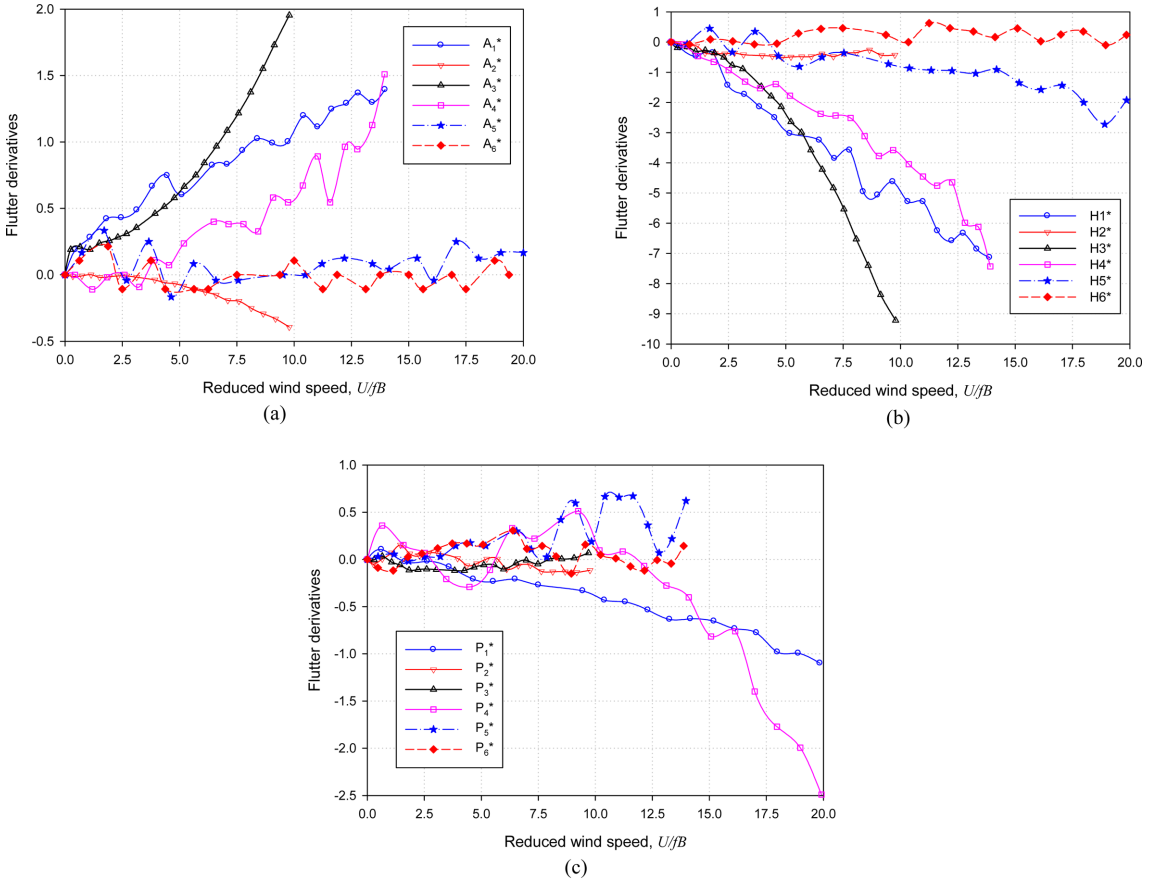

Fig. 8 Experiment flutter derivatives for the New Millennium Bridge: (a) $A_i^*(i=\overline{1,6})$, (b) $H_i^*(i=\overline{1,6})$, (c) $P_i^*(i=\overline{1,6})$

bridge model have been conducted by the Daewoo Institute of Construction Technology (DICT). A distinct feature of the bridge is it's high (195.0 m) and low (135.0 m) pylons with two bundle cables in the rear span (Kim *et al.* 2010). A constant modal damping ratio of critical ζ = 0.34% is suggested for the section model tests. Fig. 7 shows that the bridge section has a streamlined steel box with a 16.1 m width and a 2.6 m height.

The wind tunnel tests were performed on a three degree-of-freedom elastically suspended section model for extracting the experimental flutter derivatives, A_i^*, H_i^* and $P_i^*(i=\overline{1,6})$; the results are shown in Fig. 8. The structure is modeled by a three-dimensional framework with a total of 656 nodes, 772 elements (space beams, cables, and rigid links) and 279 nodal masses.

To verify the reliability and utility of the propose method, the cable is modeled with two different elements: truss element (called analysis I) and proposed spatial catenary cable element (called analysis II). In the analysis I, the sagging of the inclined cables is to consider an equivalent straight chord member with an equivalent modulus of the elasticity, as suggested by Ernst (1965). To do vibration finite element and aerodynamic bridge analysis, consistent and lumped mass matrices of individual elements for analysis I and analysis II, respectively, are employed. Numerical results

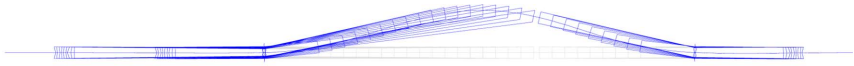

Plan Mode shape 1

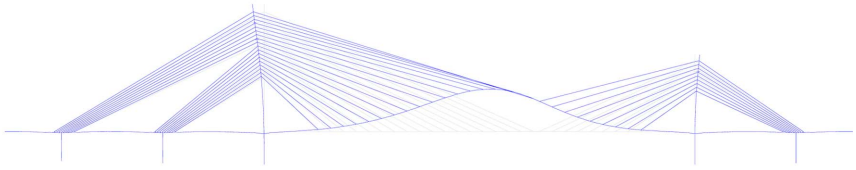

Elevation Mode shape 2

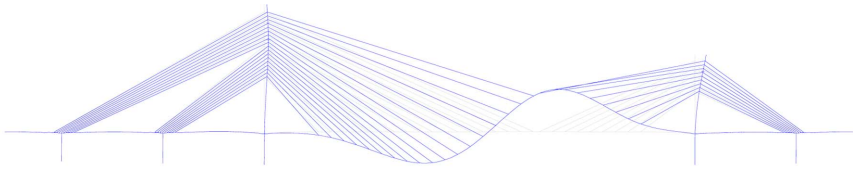

Elevation Mode shape 4

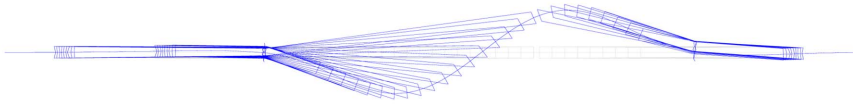

Plan Mode shape 6

Fig. 9 Fundamental mode shapes of the New Millennium bridge

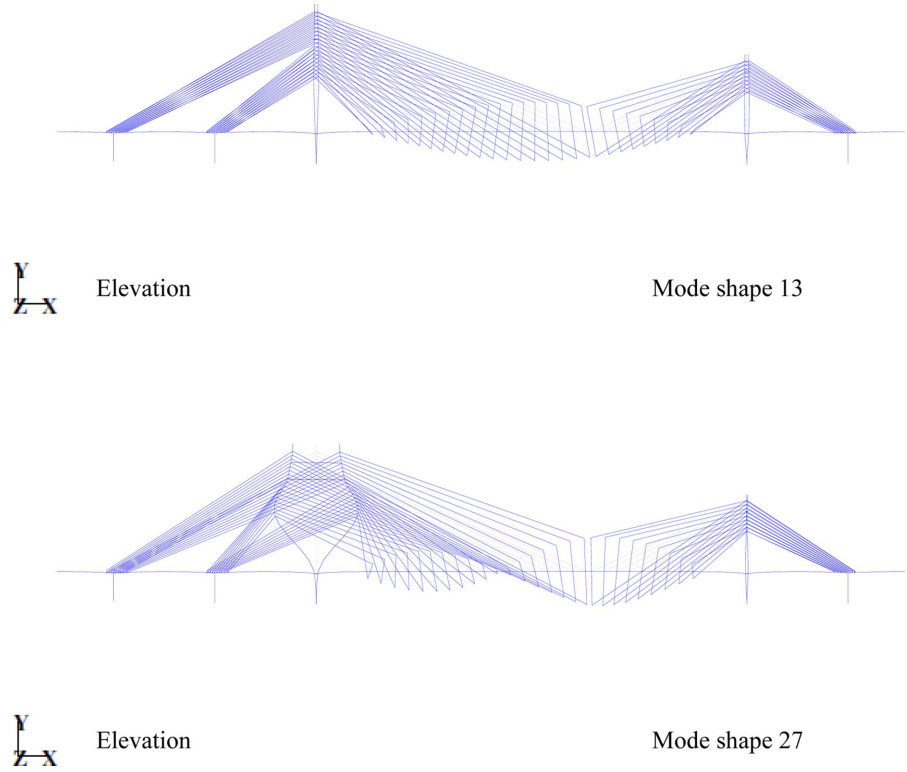

Fig. 9 Continued

derived from the MIDAS commercial software are used as reference solutions to assess the agreement of the proposed codes.

From the free vibration analysis, some of the fundamental mode shapes of the cable-stayed bridge are presented in Fig. 9. The natural frequencies and mode shapes for the first 30 modes are shown in Table 6, and are essential for the analysis of the aerodynamic instability of the bridge under laminate wind flow approaches. Table 6 also shows the discrepancy between the results of analysis I and that of analysis II, which is less than 1.5%. It should be noted that both results are agreed well with those given by the MIDAS commercial software.

Based on the multi-mode flutter algorithm using 18 flutter derivatives expressed in a complex form as described in section 3, the coupled flutter problem of the New Millennium Bridge is analyzed by performing a series of complex-eigen analyses, wherein the reduced frequency varies from 0.20 to 1.07 while using a step of 2.5×10^{-3}. According to the results, multiple intersection points may occur, showing the theoretical instability at a certain reduction of frequency.

The critical condition of flutter instability is that in which an eigenvalue that is characterized by the real part passes to the zero point from the negative to the positive part, and the imaginary part becomes the corresponding frequency. The critical wind velocity for flutter should be a minimum value corresponding to its frequency. It is observed that two possible critical flutter states are found; however, the onset flutter was estimated at $U_{f2} = 82.11$ m/s and $\omega_{f2} = 2.142$ rad/s.

In order to illustrate the pre-flutter and post-flutter behavior of the cantilevered structure, a diagram illustrates the real part (logarithmic decrement σ_j) versus the imaginary part (oscillation

Table 6 Comparison of natural frequencies and mode shapes of the New Millennium Bridge

Mode No.	Natural frequency ω (rad/s)				Mode shape
	MIDAS	Analysis I	Analysis II	Error $\Delta\omega$ (%)	
1	1.650	1.677	1.693	-0.96	L-S-1
2	1.968	1.975	1.981	-0.31	V-S-1
3	2.782	2.849	2.851	-0.07	HT-L-A-1*
4	2.845	2.876	2.869	0.27	V-A-1
5	3.723	3.728	3.723	0.13	V-S-2
6	4.105	4.181	4.175	0.14	L-A-1
7	4.468	4.664	4.649	0.31	LT-L-A-1*
8	4.651	4.790	4.775	0.31	V-A-2
9	5.434	5.458	5.430	0.51	V-A-3
10	5.735	5.929	5.848	1.36	LS-L-S-1*
11	6.041	6.060	6.041	0.31	V-S-3
12	6.987	6.963	6.944	0.28	V-A-4
13	7.112	7.071	7.011	0.85	T-S-1
14	7.184	7.184	7.184	0.00	V-A-5
15	7.506	7.388	7.357	0.42	T-S-2
16	7.512	7.499	7.470	0.39	V-A-6
17	8.299	8.080	8.047	0.41	V-S-4
18	8.563	8.551	8.552	-0.02	SS-V-S-1*
19	8.709	8.930	8.821	1.22	SS-L-S-1*
20	9.071	9.092	9.059	0.37	V-S-5
21	9.577	9.585	9.585	0.00	LS-V-S-1*
22	9.701	10.145	10.022	1.22	LS-L-A-2*
23	10.117	10.196	10.145	0.50	HT-L-A-2*
24	10.986	11.045	11.004	0.38	L-A-2*
25	11.016	11.348	11.296	0.46	V-A-7
26	11.206	11.670	11.648	0.19	HT-L-S-1*
27	12.983	12.776	12.685	0.72	T-A-1
28	13.246	13.172	13.090	0.62	T-A-2
29	13.475	13.448	13.397	0.38	V-S-6
30	14.571	14.102	14.052	0.36	V-A-8

frequency ω_j) corresponding to the range of the reduced frequency K_j as shown in Fig. 10 for the case of the multi-mode flutter analysis, which is based on the first 30 modes of this structure.

Table 7 shows a comparison of the flutter wind velocity and critical frequency predicted by both analysis I, analysis II and the Ding *et al.*, methods (2002) with those measured from the aeroelastic

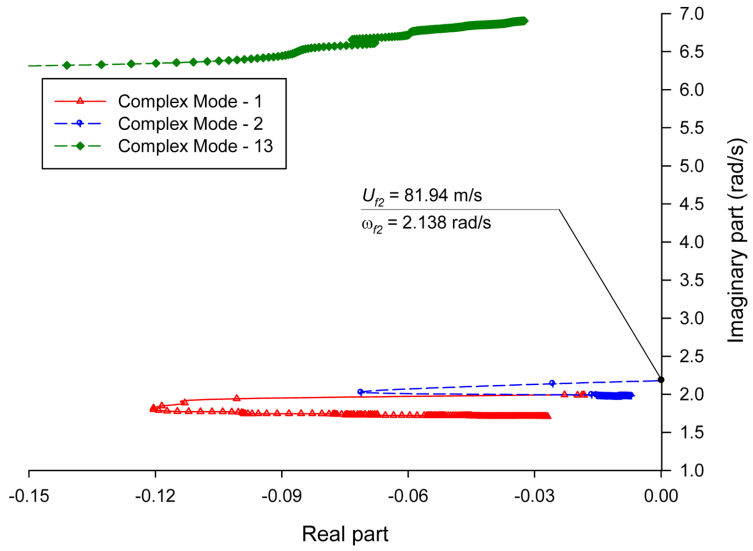

(a) Fundamental modes (1st Lateral, Vertical,Torsional mode)

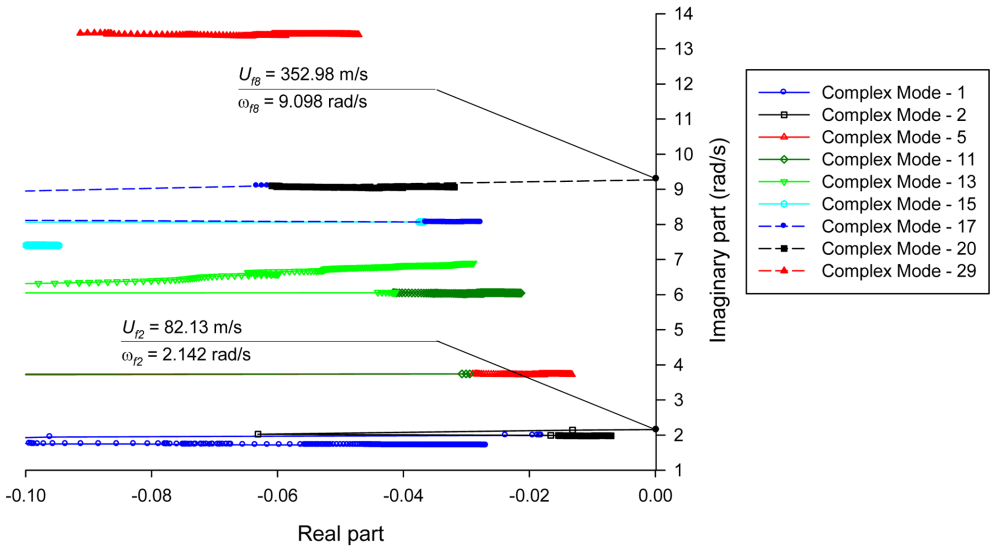

(b) Sysmetrical modes

Fig. 10 Flutter eigenvalue evolution of the New Millennium Bridge

full model test for the bridge in service stage (Kim *et al.* 2010). The use of the multi-mode flutter analysis procedure based on analysis II predicts the flutter speed of 82.11 m/s and critical frequency of 2.142 rad/s, which are in good agreement with other methods and the value of the flutter speed is also very close to the experimental result.

Table 7 Flutter analysis results by using contributed modes for the New Millennium Bridge

Reference	Contributed modes	Error ΔU (%)	Flutter velocity U_f (m/s)	Critical frequency ω (rad/s)
Analysis I	Fundamental modes (1,2,13)	-3.11	81.46	2.125
	Sysmetrical modes (1,2,5,11,13,15,17,20,29)	-2.80	81.71	2.132
	First 30 modes	-2.82	81.70	2.131
Analysis II	Fundamental modes (1,2,13)	-2.52	81.94	2.138
	Sysmetrical modes (1,2,5,11,13,15,17,20,29)	-2.28	82.13	2.142
	First 30 modes	-2.30	82.11	2.142
Ding *et al.* (2002)	First 30 modes	-7.29	78.29	2.042
Wind tunnel tests (Kim *et al.* 2010)	-	-	84.00	-

6. Conclusions

In this article, a spatial catenary cable element has been presented for the analysis of cable-supported and tension structures. The derivation is based on the exact analytical expressions of the elastic catenary. The self weights of the cables are included accurately without any assumptions, and the element stiffness matrix and the end forces are calculated based on the iteration procedures. The prestress state in the cable element is also considered. Furthermore, an iterative algorithm for form-finding of cables is proposed to determine their original lengths, which are definitely balanced in the initial geometrical conditions as well as the pretensioned forces. Numerical comparisons with results obtained by the other formulations of other cable elements or available experimental evidences show the effectiveness and efficiency of the spatial catenary cable element.

References

Andreu, A., Gil, L. and Roca, P. (2006), "A new deformable catenary element for the analysis of cable net structures", *Comput. Struct.,* **84** (29-30), 1882-1890.

Ali, H. and Abdel-Ghaffar, A. (1995), "Modeling the nonlinear seismic behavior of cable- stayed bridges with passive control bearings", *Comput. Struct.,* **54**(3), 461-492.

Argyris, J. and Scharpf, D. (1972), "Large deflection analysis of prestressed networks", *J. Struct. Div.*, *ASCE*, **98**(3), 633-654.

Cohen, E. and Perrin, H. (1957), "Design of multi-level guyed towers: analysis", *J. Struct. Div., ASCE*, **83**, 1356.1.

Coyette, J. and Guisset, P. (1988), "Cable network analysis by a nonlinear programming technique", *Eng. Struct.*, **10**(1), 41-46.

Chen, Z.H., Wu, Y.J., Yin, Y. and Shan, C. (2010), "Formulation and application of multi-node sliding cable element for the analysis of Suspend-Dome structures", *Finite Elem. Anal. D.*, **46**(9), 743-750.

Ding, Q.S., Chen, A.R. and Xiang, H.F. (2002), "Coupled flutter analysis of long-span bridges by multimode and full-order approaches", *J. Wind Eng. Ind. Aerodyn*., **90**, 1981-1993.

Ernst, H. (1965), "Der E-modul von seilen unter beruecksichtigung des durchhanges", *Der Bauingenieur*, **40**(2), 52-55. (in German)
Gambhir, M. and Batchelor, B. (1977), "A finite element for 3-D prestressed cable nets", *Int. J. Numer. Meth. Eng.,* **11**(11), 1699-1718.
Gambhir, M. and Batchelor, B. (1979), "Finite element study of the free vibration of a 3-D cable networks", *Int. J. Solids Struct.*, **15**(2), 127-136.
Jain, A., Jones, N.P. and Scanlan, R.H. (1996), "Coupled aeroelastic and aerodynamic response analysis of long-span bridges", *J. Wind Eng. Ind. Aerod.,* **60**, 69-80.
Jayaraman, H. and Knudson, W. (1981), "A curved element for the analysis of cable structures", *Comput. Struct.*, **14**(3-4), 325-333.
Karoumi, R. (1999), "Some modeling aspects in the nonlinear nite element analysis of cable supported bridges", *Comput. Struct.*, **71**, 397-412.
Kim, D.Y., Kim, H.Y., Kim, Y.H., Kwak, Y.H., Park, J.G. and Shin, S.H. (2010), "Wind engineering studies for the New Millennium Bridge (1st Site)", Technical Report, DAEWOO Institute of Construction Technology, South Korea.
Krishna, P. (1978), *Cable-suspended Roofs*, McGraw-Hill, New York.
Kwan, A. (1998), "A new approach to geometric nonlinearity of cable structures", *Comput. Struct.*, **67**(4), 243-252.
Lewis, W., Jones, M. and Rushton, K. (1984), "Dynamic relaxation analysis of the non-linear static response of pretensioned cable roofs", *Comput. Struct.*, **18**(6), 989-997.
Liu, H. and Chen, Z. (2012), "Structural behavior of the suspen-dome structures and the cable dome structures with sliding cable joints", *Struct. Eng. Mech.,* **43**(1), 53-70.
Michalos, J. and Birnstiel, C. (1960), "Movements of a cable due to changes in loading". *J. Struct. Div., ASCE*, **86**(12), 23-38.
Mollmann, H. (1970), "Analysis of plane prestressed cable structures", *J. Struct. Div.*, *ASCE*, **96**, 2059.
O'Brien, W. and Francis, A. (1964), "Cable movements under two-dimensional loads", *J. Struct. Div.*, *ASCE*, **90**(3), 89-123.
Ozdemir, H. (1979), "A finite element approach for cable problems", *Int. J. Solids Struct.*, **15**(5), 427-437.
Peyrot, A.H. and Goulois, A.M. (1978), "Analysis of flexible transmission lines", *J. Struct. Div., ASCE*, **104**, 763-779.
Peyrot, A.H. and Goulois, A.M. (1979), "Analysis of cable structures", *Comput. Struct.*, **10**(5), 805-813.
Poskitt, T.J. and Livesley, R.K. (1963), "Structural analysis of guyed masts", *Proc. Inst. Civ. Eng.*, **14**, 373.
Saafan, S.A. (1970), "Theoretical analysis of suspension roofs", *J. Struct. Div.*, *ASCE*, **96**(2), 393-404.
Sarkar, P.P., Jones, N.P. and Scanlan, R.H. (1994), "Identification of aeroelastic parameters of flexible bridges", *J. Eng. Mech.*, *ASCE*, **120**(8), 1718-1742.
Starossek, U. (1998), "Complex notation in flutter analysis", *J. Struct. Eng.*, *ASCE*, **124**(8), 975-977.
Such, M., Jimenez-Octavio, J.R., Carnicero, A. and Lopez-Garcia, O. (2009), "An approach based on the catenary equation to deal with static analysis of three dimensional cable structures", *Struct. Eng.*, **31**(9), 2162-2170.
Sufian, F.M.A. and Tempelman, A.B. (1992), "On the non-linear analysis of pre-tensioned cable net structures", *Struct. Eng.*, **4**(2), 147-158.
Tibert, G. (1998), *Numerical Analyses of Cable Roof Structures*, Royal Institute of Technology, Dept. of Structural Engineering.
Vu, T.V. (2010), "Aeroelastic flutter analysis of long-span bridges", Ph.D. dissertation, Korea University, South Korea.
Vu, T.V., Kim, Y.M., Lee, H.Y., Yoo, S.Y. and Lee, H.E. (2011), "Flutter analysis of bridges through use of by state space method", *Proceedings of the 8th Int. Conf. Struct. Dyn.*, EURODYN 2011, Belgium, 3083-3090.
Wang, C., Wang, R., Dong, S. and Qian, R. (2003), "A new catenary cable element", *Int. J. Space Struct.*, **18**(4), 269-275.
West, H.H. and Kar, A.K. (1973), "Dicretized initial-value analysis of cable nets", *Int. J. Solids Struct.*, **9**, 1403-1420.
Yang, Y.B. and Tsay, J.Y. (2007), "Geometric nonlinear analysis of cable structures with a two-node cable element by generalized displacement control method", *Int. J. Struct. Stab. Dyn.*, **7**(4), 571-588.